

Scattering of Evanescent Wave by Periodic Array of Nanowires

Leonid L. Frumin,^{1,2} Anton V. Nemykin,^{1,2} Sergey V. Perminov,³ and David A. Shapiro^{1,2,4}

¹*Institute of Automation and Electrometry, Siberian Branch,
Russian Academy of Sciences, Novosibirsk 630090, Russia*

²*Novosibirsk State University, Novosibirsk 630090, Russia*

³*A.V. Rzhanov Institute of Semiconductor Physics, Siberian Branch,
Russian Academy of Sciences, Novosibirsk 630090, Russia*

⁴*Corresponding author: shapiro@iae.nsk.su*

The scattering of electromagnetic wave by a periodic array of nanowires is calculated by the boundary element method. The method is extended to the infinite grating near the interface between two dielectrics. A special Green function is derived that allows to study the evanescent wave. The Rayleigh—Wood's anomalies are found in the period-to-wavelength dependence of the average Poynting vector in the wave zone. For thin wires the calculations are shown to agree with the two-dimensional coupled dipole approximation.

PACS numbers: 42.25.Fx,42.25.Gy,02.70.Pt

I. INTRODUCTION

The travelling wave falling onto the boundary between two dielectrics by the angle of total internal reflection generates an evanescent wave in the second medium. The illumination by evanescent wave is widely used in applications. In near-field scanning optical microscopy it allows one to detect the desired signal with no background [1]. Total internal reflection fluorescence, exploiting decay of evanescent wave, achieves nanometer resolution along the optical path through a thin object [2]. Covering the fiber surface by nanowires improves the sensitivity of fiber Bragg grating refractometry [3].

While the scattering problem for evanescent wave is of importance, it has, however, no analytical solution. The necessity of treating the evanescent wave along with its source exaggerates the calculation. For travelling wave the analytical solution exists for the homogeneous medium and one circular cylinder [4]. The numerical methods allows one to solve the problem for one elliptic cylinder [5]. The numerical solution for two different dielectric half spaces are found recently for one [6] and two [7] cylinders. The scattering by few cylinders has very small cross-section and then is difficult to observe. To enhance the effect one needs to consider a number of cylinders, but growing the number of scatterers results in additional computational difficulty. To remedy this contradiction between the observation needs and computation difficulties, we reduce a two-dimensional infinite periodic array to only one unit cell with the help of periodicity. The aim of the present paper is to calculate the scattering of evanescent wave by the periodic array of parallel cylinders of arbitrary diameter.

The periodic structures of scatterers with subwavelength dimension of each enhance the signal compared to one scatterer [8–10]. Two-dimensional structures are important, for instance, for photonic crystals [11] or metamaterials [12]. The diffraction grating can be characterized by its Rayleigh — Wood’s anomalies. We consider these resonances and compare their structure with the case of travelling wave and with widely used coupled dipole approximation.

For this purpose we propose a modification of the boundary integral equations, Section II, which are the basis of the Boundary Element Method (BEM) [13–15]. We derive a special Green function that takes into account the evanescent wave together with its source, the dielectric half-space, in Subsection II A. The method is extended to the periodic array in

Subsection II B. In Section III we present the results of calculation. Subsection III A contains the study of average energy flux in the far-field domain as a function of period-to-wavelength ratio, including splitting of Rayleigh— Wood’s anomalies. The Subsection III B is devoted to the calculation within dipole approximation, in comparison to the more rigorous BEM, for the travelling exciting wave. The coupled dipoles equations are presented for both finite and infinite periodic grating.

II. METHOD

A. Green Function

Let us consider two media, 1 and 2, separated by a plane boundary at $y = 0$. We look for the specific Green function $G(x, y; x', y')$ satisfying inhomogeneous equation

$$\Delta G + k^2 G = \delta(x - x')\delta(y - y') \quad (1)$$

in these media. Function G depends on the difference $x - x'$ only due to translational symmetry. The boundary condition at $y = 0$ for p -wave is

$$[G(x, y; x', y')]_{y=0} = \left[\frac{1}{\varepsilon} \frac{\partial G(x, y; x', y')}{\partial y} \right]_{y=0} = 0. \quad (2)$$

After the Fourier transformation

$$G(x, y; 0, y') = \frac{1}{2\pi} \int_{-\infty}^{\infty} G_q(y, y') e^{iqx} dq \quad (3)$$

Eq. (1) is reduced to an ordinary differential equation having exponential solutions. Using conditions (2) we obtain the function. The expression for $y' > 0$ in q -domain is

$$G_q = -\frac{1}{2\mu_2} \begin{cases} [1 + r(q)] e^{\mu_1 y - \mu_2 y'}, & y < 0, \\ e^{-\mu_2 |y - y'|} + r(q) e^{-\mu_2 (y + y')}, & y > 0. \end{cases} \quad (4)$$

Here

$$r(q) = \frac{\varepsilon_1 \mu_2 - \varepsilon_2 \mu_1}{\varepsilon_1 \mu_2 + \varepsilon_2 \mu_1} \quad (5)$$

is the Fresnel reflection coefficient of p -wave at normal incidence [16], $\mu_{1,2}^2 = q^2 - k_{1,2}^2$.

Carrying out Fourier transformation (3) of function (4) at $y > 0$ we have two terms

$$G_1 = - \int_{-\infty+i0}^{\infty-i0} e^{-\mu_2|y-y'|+iq(x-x')} \frac{dq}{4\pi\mu_2}, \quad (6)$$

$$G_2 = - \int_{-\infty+i0}^{\infty-i0} e^{-\mu_2(y+y')+iq(x-x')} \frac{r(q) dq}{4\pi\mu_2}, \quad (7)$$

where $G = G_1 + G_2$. The sign of the square root is given by the rule $\sqrt{q^2 - k_2^2} \rightarrow -i\sqrt{k_2^2 - q^2}$, $q^2 < k_2^2$.

The first term (6) can be calculated analytically and reduces to the known Green function of Helmholtz equation in the homogeneous space

$$G_1(\vec{r}; \vec{r}') = \frac{1}{4i} \mathcal{H}_0^{(1)}(k_2 \rho_-), \quad (8)$$

where $\mathcal{H}_0^{(1)}$ denotes the Hankel function of the first kind [17],

$$\rho_{\pm} = \sqrt{(x-x')^2 + (y \pm y')^2} \quad (9)$$

are the distances from the source and its image. The second term G_2 gives the effect of the reflected image source. The amplitude of the source at each q is equal to the reflection coefficient $r(q)$. Thus along with the point source at (x', y') we have to consider mirror-image source $r(q)$ at $(x', -y')$. The total field at the upper half-plane is the sum of the fields generated by the two sources at each q . This approach intrinsically takes into account the multiple scattering. The Green function of this type was studied for homogeneous waves: spherical acoustic, see [18, 19], or cylindrical electromagnetic waves [20]. A general approach has been built, based on integral equation, to study the field scattered by an object near two-media interface, for excitation by homogeneous [21] and evanescent [6, 7] light wave.

Analogous calculations give the Green function for the source inside the lower dielectric.

$$G_q = -\frac{1}{2\mu_1} \begin{cases} e^{-\mu_1|y-y'|} - r(q)e^{\mu_1(y+y')}, & y < 0, \\ [1 - r(q)]e^{-\mu_2 y + \mu_1 y'}, & y > 0. \end{cases} \quad (10)$$

Comparing function (10) with (4) we see that the expression can be obtained by the symmetry transformation, namely, changing medium indices $1 \leftrightarrow 2$ and the sign of the ordinate $y \rightarrow -y$, $y' \rightarrow -y'$. The case of s -wave the boundary conditions (2) are replaced by

$$[G(x, y; x', y')]_{y=0} = \left[\frac{\partial G(x, y; x', y')}{\partial y} \right]_{y=0} = 0. \quad (11)$$

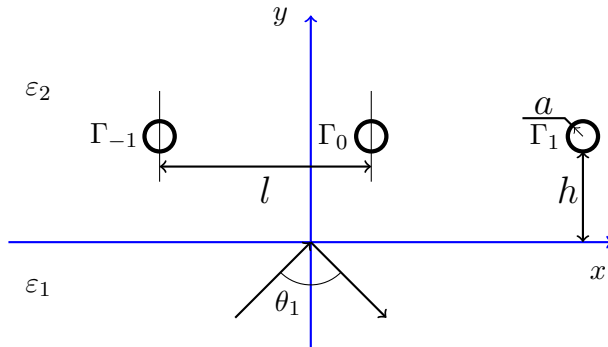


FIG. 1. A cross-section of the periodic array of cylinders: a is the radius, h is the gap, l is the period, θ_1 is the light incidence angle.

The result can be also obtained from (4) replacing the Fresnel reflection coefficient (5) for normal incidence by its expression for s -wave

$$r(q) = \frac{\mu_2 - \mu_1}{\mu_1 + \mu_2}. \quad (12)$$

The compound Green function is valid in both half-spaces and makes it possible to solve the scattering problem near the interface between two dielectrics. This function is yet for few cylinders but worthless for the periodic grid. In the next section we explain how to extend the computation for the infinite grid with the help of Floquet theorem and derive the corresponding effective Green function.

B. Boundary Element Method

Let us consider a scattering of a plane wave by the periodic grid of identical parallel cylinders with dielectric permittivity ε_3 , see Fig. 1. The grid is located in dielectric half-space 2 (with dielectric permittivity ε_2) parallel to its boundary with half-space 1 (ε_1). A travelling wave with frequency ω falls from half-space 1 by the angle of incidence θ_1 . Denote $k_{1,2} = k_0\sqrt{\varepsilon_{1,2}}$ the wavenumber in each dielectric, where $k_0 = \omega/c$, c is the speed of light. As known from Fresnel formulas, the transmitted wave in media 2 becomes evanescent when angle θ_1 exceeds the angle of total internal reflection. Choose axis z along the axes of cylinders, axis x along the boundary, and axis y perpendicular to the boundary, as shown in Fig. 1.

We concentrate on the p-wave (TM case), when the magnetic field has only z -component, which consists of the falling and the scattered fields: $H_z = H_0 + H'$. With the help of integral

Green formula we write the coupled boundary integral equations for scattered field $u = H'$ and its normal derivative $f = \partial H' / \partial n$ at a contour point $P = (x, y) \in \Gamma$:

$$-\frac{u(P)}{2} + \int_{\Gamma} \left[\frac{\partial G_{\text{out}}}{\partial n_Q} u(Q) - G_{\text{out}} f(Q) \right] dQ = 0. \quad (13)$$

Here n_Q is the internal normal in point $Q = (x', y') \in \Gamma$, $G_{\text{out}}(P, Q)$ is the external Green function. The integration point Q runs through compound contour $\Gamma = \cup_m \Gamma_m$, where Γ_m is the contour of m -th circle (cross section of cylinder): $m = 1, 2, \dots, N$; N is the number of cylinders. The integral over an unlinked domain is a sum of integrals over partial contours Γ_m . This equation corresponds to the outer limit, i.e. the limit of Green formula when the observation point tends to contour Γ from the external side. For the outer limit we use the special Green function described in Sec. II A. It explicitly takes into account the boundary conditions at the plane interface between the dielectrics 1 and 2, and has a form of divergent wave at infinity [6, 7].

The second integral equation arises as a result of the passage to the inner limit, i.e. when point P tends to the contour from internal area:

$$\frac{u(P)}{2} + \int_{\Gamma_m} \left[\frac{\partial G_{\text{in}}}{\partial n_Q} u(Q) - G_{\text{in}} f(Q) \right] dQ = B_0, \quad (14)$$

$$B_0 = -\frac{u_0}{2} - \int_{\Gamma_m} \left(\frac{\partial G_{\text{in}}}{\partial n} u_0 - G_{\text{in}} f_0 \right) dQ. \quad (15)$$

Here $G_{\text{in}}(P, Q)$ is the internal Green function, $u_0 = H_0$, $f_0 = \partial H_0 / \partial n$. For internal domain we use the cylindrical wave

$$G_{\text{in}}(x, y; x', y') = \frac{1}{4i} \mathcal{H}_0^{(1)}(k_3 \rho_-). \quad (16)$$

For N cylinders there are N internal and N external equations. Solving the set of $2N$ equations we find functions $u(P), f(P), P \in \Gamma$. If we know functions u, f at the contour, then scattered field in arbitrary external point $R = (x, y) \notin \Gamma$ can be found from the Green theorem

$$u(R) = \int_{\Gamma} \left[\frac{\partial G_{\text{out}}}{\partial n_Q} u(Q) - G_{\text{out}} f(Q) \right] dQ, \quad (17)$$

where $G_{\text{out}} \equiv G_{\text{out}}(R, Q)$ is the external Green function.

Eqs. (13), (14) refer to the case of a finite number N of the cylinders. Passing to the limit $N \rightarrow \infty$ we consider points at the compound contour with equal $y_m = y_0$ and $x_m = x_0 + ml; m = 0, \pm 1, \pm 2, \dots$. A zeroth cylinder $m = 0$ is chosen arbitrary for the infinite

grating. The following property (also known as Floquet theorem) is a consequence of the periodicity:

$$u(x_m, y_m) = u(x_0 + md, y_0) = u(x_0, y_0)e^{ik_\perp ml}, \quad (18)$$

where $k_\perp = k_1 \sin \theta_1$ is the tangential component of the wavevector conserved at the boundary. Taking into account the same property of function $f(Q)$ and reversing the order of summation and integration in Eq. (13) and (17)[22] we obtain the sum:

$$\sum_{m=-\infty}^{+\infty} \left[\frac{\partial G_{\text{out}}}{\partial n_Q} u(Q) - G_{\text{out}} f(Q) \right] e^{ik_\perp ml}. \quad (19)$$

The special Green function (3), (4) in the upper half space 2 can be written as a contour integral

$$G_{\text{out}} = - \int_C \left(e^{-\mu|y-y'|} + r_k e^{-\mu(y+y')} \right) \frac{e^{ik\Delta} dk}{4\pi\mu}, \quad (20)$$

where $y, y' > 0$, $\Delta = x - x'$, $G_{\text{out}} \equiv G_{\text{out}}(x, y; x', y')$, $\mu = \sqrt{k^2 - k_2^2}$, $C = (-\infty + i0, +\infty - i0)$. Consider the latter sum in Eq. (19)

$$G_{\text{eff}} = \sum_{m=-\infty}^{+\infty} G_{\text{out}}(x, y; x'_m, y'_m) e^{ik_\perp ml}. \quad (21)$$

From (21) and integral representation (20), alternating the order of summation and integration, we obtain the periodic delta function

$$\sum_{m=-\infty}^{+\infty} e^{-ikmd + ik_\perp md} = \frac{2\pi}{l} \delta(k - k_\perp - n\kappa), \quad (22)$$

where $n = 0, \pm 1, \pm 2, \dots$, $\kappa = 2\pi/l$ is the reciprocal lattice vector. Then integrating the delta-function over k we get the expression for G_{eff}

$$G_{\text{eff}} = - \sum_{n=-\infty}^{+\infty} \frac{e^{i(k_\perp + n\kappa)\Delta_0}}{2l\mu_n} \left[e^{-\mu_n|y-y'_0|} + r_n e^{-\mu_n(y+y'_0)} \right], \quad (23)$$

where $\Delta_0 = x - x'_0$, $\mu_n = \sqrt{(k_\perp + n\kappa)^2 - k_2^2}$, $r_n = r_{k_\perp + n\kappa}$. The former term in Eq. (19) is reduced to the normal derivative of (23) analogously, changing the order of normal derivative and summation.

Expression (23) determines the effective Green function, taking into account the infinite grid as a whole. If we replace G_{out} by G_{eff} in external integral equation (13) and Green theorem (17), then the path of integration will be Γ_0 . It is the zeroth circle, the connected

contour, instead of infinite unlinked contour Γ . Only one internal equation should be solved, for $m = 0$. After finding functions $u(P), f(P)$ we use Eq. (17) for calculation of the field in the wave zone.

III. RESULTS

A. Rayleigh — Wood's anomalies

We study the transparency of the grating as a function of distance l between the neighbor cylinders. The transparency is defined as a ratio of y -projection of average Pointing vector to the energy flux density of the falling wave. The Pointing vector is averaged over the period and calculated at sufficiently large distance from the boundary $y \sim 10\lambda$, where $\lambda = 1.5 \mu\text{m}$ is the fixed wavelength.

Only terms corresponding to travelling waves with $(k_{\perp} + n\alpha)^2 < k_2^2$ (and then $\text{Re}\mu_n = 0$) have to be kept for calculations in the wave zone. Thus, the sum (23) becomes finite and relatively easy for numerical calculation compared to integral representation (20). Fig. 2 shows the transparency as a function of the spacing between the cylinders, l , (rated to the wavelength) for the travelling wave ($\varepsilon_1 = \varepsilon_2 = 1, \theta_1 = 45^\circ$). The grating is placed close to the surface: $h = 0.01 \mu\text{m}$.

We see the narrow dips, so-called Rayleigh — Wood's anomalies (RWA). These resonances take place when the grazing mode appears. The condition of resonance is synchronization of the phases between the waves scattered by neighbor cylinders. The grazing modes may have both positive and negative order $n = \pm 1, \pm 2, \dots$. The positive orders $n > 0$ generate the surface wave going in negative direction and vice versa. For positive/negative mode the synchronism condition is

$$k_1 l \sin \theta_1 \pm k_2 l = 2\pi|n|. \quad (24)$$

Here $k_1 l \sin \theta_1$ is the difference of optical paths in half-space 1, $k_2 l$ is the difference in half-space 2. The expression (24) is valid only for small diameters $2a \ll \lambda$.

Let us express the wavenumbers in terms of the wavelength $k_{1,2} = 2\pi\sqrt{\varepsilon_{1,2}}/\lambda$. Eq. (24) can be rewritten as

$$\frac{l}{\lambda} = \frac{\pm|n|}{\sqrt{\varepsilon_1} \sin \theta_1 \pm \sqrt{\varepsilon_2}}. \quad (25)$$

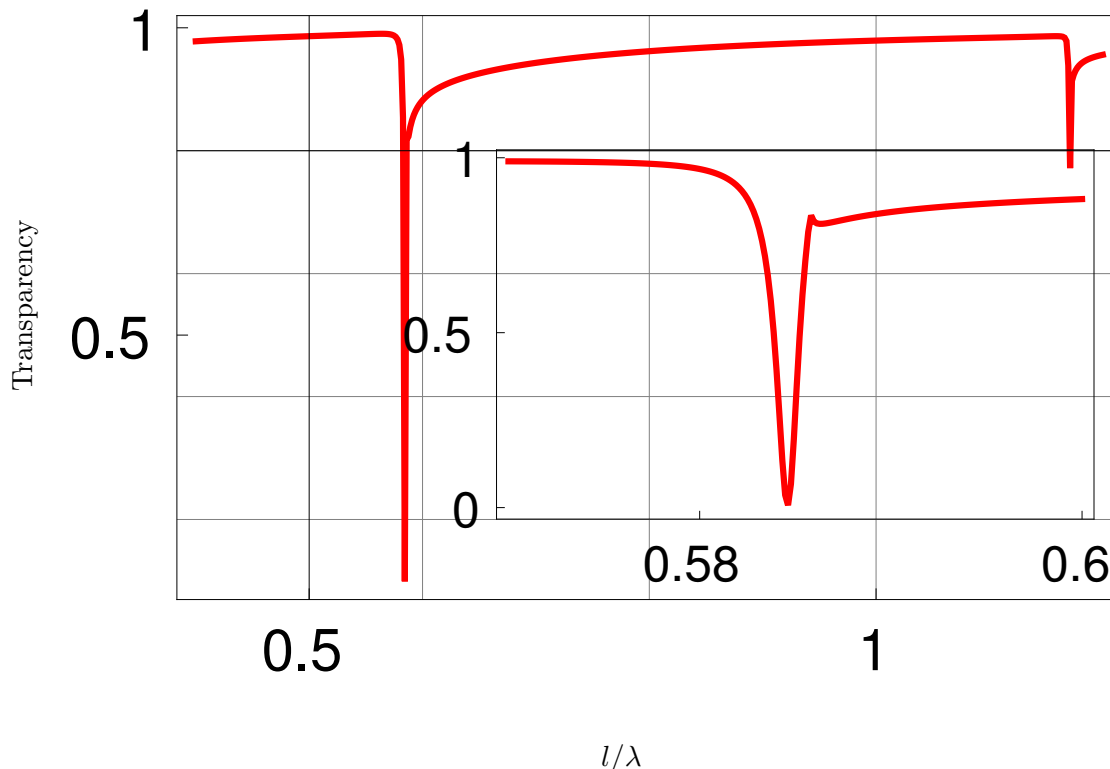


FIG. 2. Raleigh — Wood’s anomalies in the transparency for travelling wave ($\epsilon_1 = 1$, the cylinders’ radii $a = 0.1 \mu\text{m}$). The first dip with higher resolution is shown in the inset.

In vacuum for $n = 1, 2$ and $\theta_1 = 45^\circ$ it gives $l/\lambda = 0.5858, 1.1716, \dots$. Near the resonance a rearrangement of the wave pattern occurs due to arising the next order diffraction and transparency decreases sharply. The inset demonstrates the splitting of the first dip. Its physical nature is a difference between induced dipole moments along x and y directions. This difference is verified in the section III B within the coupled dipole approximation.

The case of evanescent wave is shown in Fig. 3. The evanescent wave in the upper half space 2 arises from the travelling wave falling onto the boundary by the angle of total internal reflection (TIR). The refractive indices are $\sqrt{\epsilon_1} = 1.5, \sqrt{\epsilon_2} = 1$ (describing a glass in the air), the incident angle $\theta_1 = 45^\circ$, as above. The limit value of transparency at $l \gg \lambda$ is zero instead of unity. The positions of resonances have shifted, since in dielectric Eq. (25) gives $l/\lambda = 0.4853, 0.9706, \dots$

Comparing Fig. 2 and 3 we see an essential difference. There are four main distinctions of Fig. 3: the RWA broadening, the vanishing splitting, the weak step (“jag”) at $l/\lambda \approx 0.78$,

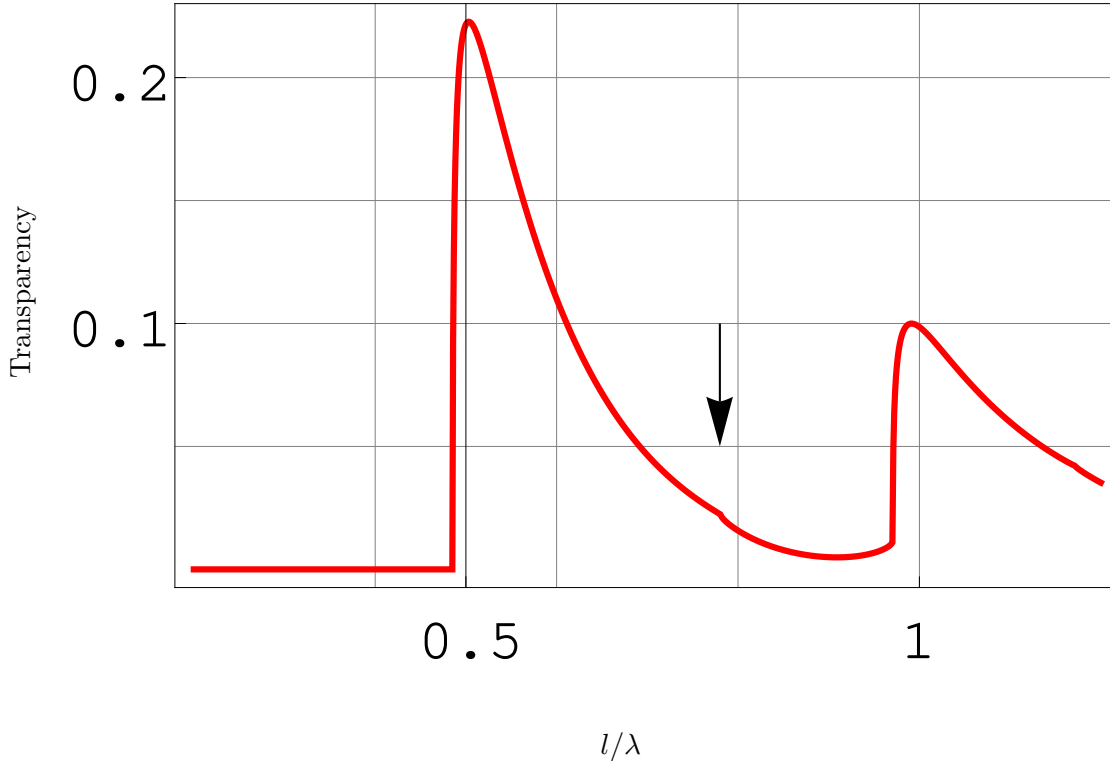


FIG. 3. The transparency as a function of period-to-wavelength ratio for evanescent wave ($\varepsilon_1 = 2.25$). An arrow indicates the weak step.

and the zero asymptotic value at $l/\lambda \rightarrow \infty$. There are two differences in conditions between Fig. 2 and 3: the dielectric lower half-space with $\sqrt{\varepsilon_1} = 1.5$ and the TIR incident angle. To clarify the contributions of both differences let us repeat the calculation for two very close angles, less and more than the TIR angle. We fix $\varepsilon_1 = 2.25, \varepsilon_2 = 1$ and choose two values in incidence angle θ_1 , both very close to the angle of total internal reflection. For our case the TIR angle is equal to $\theta_0 = \arcsin(1/\sqrt{\varepsilon_1}) = 0.729728$. Our values are $\theta_1^- \approx 0.7297$ and $\theta_1^+ \approx 0.7296$. First is less than TIR angle, the second is greater. The difference is very small, $|\theta_1^\pm - \theta_0| \approx 10^{-4}$. At the same time the angles corresponds the travelling or evanescent wave in medium 2 at almost equal conditions. The transparency curves are shown in Fig. 4. The upper curve, the transparency for travelling wave, differs noticeably from the lower one.

When the angle θ_1 is close to the TIR angle θ_0 , only RWA of positive order exist at $l/\lambda = n/2, n = 1, 2, \dots$. The travelling wave propagates nearly along the surface at x -direction and has mainly y -component of the electric field. Then the x -component of the

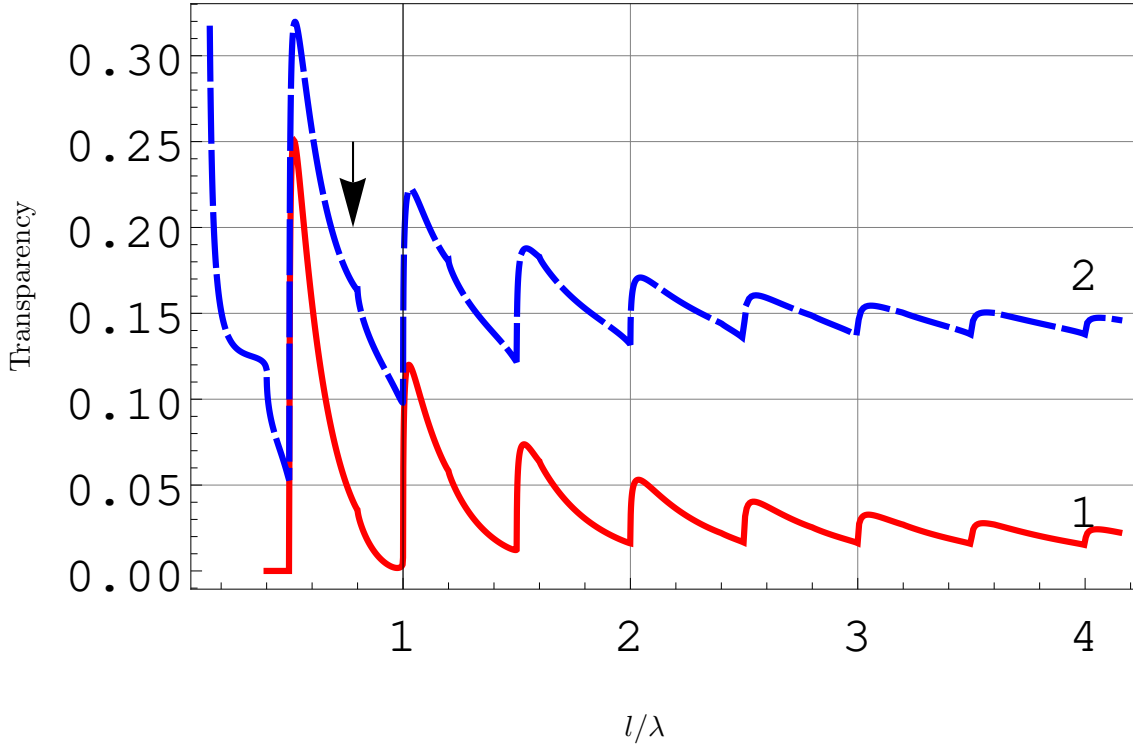


FIG. 4. The transparency as a function of period-to-wavelength ratio for a narrow gap $h = 0.01 \mu\text{m}$: the incidence angle is θ_1^+ — evanescent wave (curve 1) or θ_1^- — traveling wave (curve 2). An arrow indicates the weak step.

dipole moment is very small and the splitting vanishes. The same situation takes place for angles $\theta_1 > \theta_0$, i.e. for evanescent wave, when x -component of the dipole moment is exactly zero. Unlike, at a smaller angle θ_1 the x -component of dipole moment arises along with the RWA splitting. Also, the broadening takes place for both the curves.

The picture considerably varies also with changing the gap h . The computation in Fig. 4 correspond to $h = 10 \text{ nm}$. Fig. 5 shows the same curves for the grating placed far from the boundary, at $h = 300 \text{ nm}$, when the role of multiple reflection becomes relatively weak. In comparison with Fig. 4 the gap increasing results in higher peak values of the transparency coefficient. The step at $l/\lambda \approx 0.78$ vanishes for wide gap, and then it can be interpreted as an effect of the image source.

Thus the broadening and one component RWA are the effects of dielectric. The jag is the result of image grating reflected in the dielectric. The zero limiting value at $l/\lambda \rightarrow \infty$

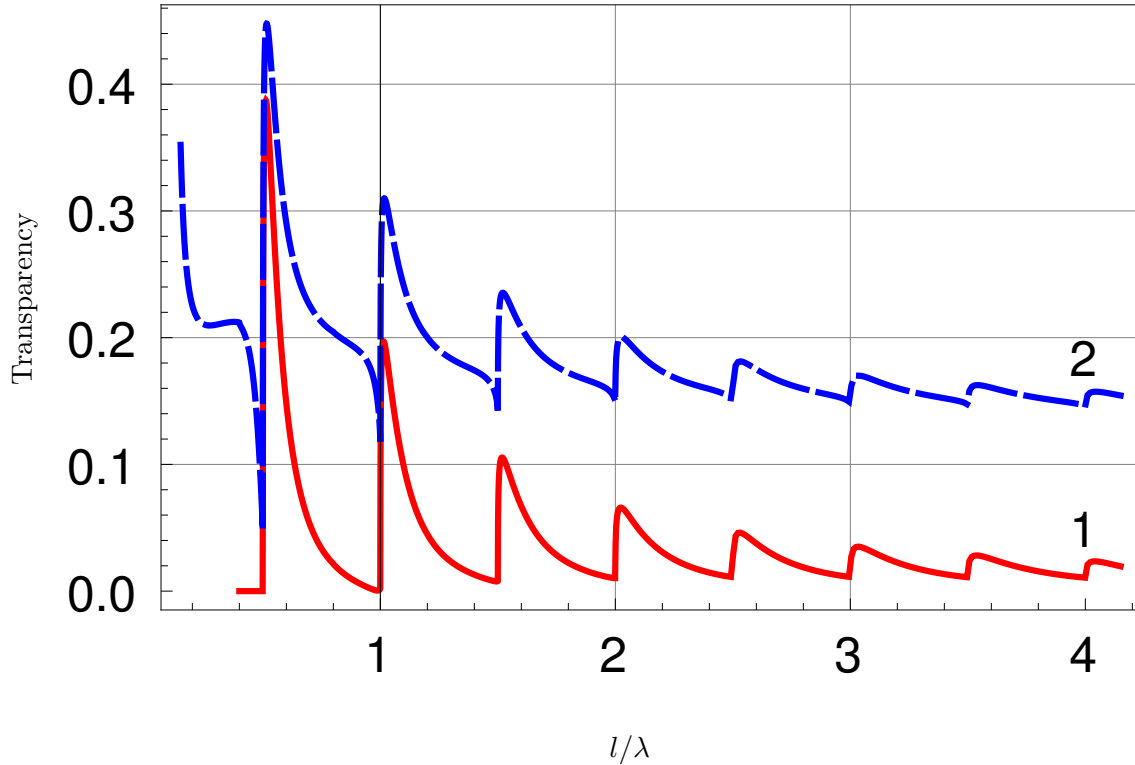


FIG. 5. The same as in Fig. 5 for the wider gap $h = 0.3 \mu\text{m}$.

is an effect of evanescent wave (zero background).

B. Discrete Dipole Approximation

In this section we consider the grid of nanowires within dipole approximation. It means that we will describe the response of the wire on the exciting electric field in terms of the wire's dipole polarizability, α . As before, we consider the case when the electric field lies in xy -plane, the acquired dipole moments are 2-dimensional. Also, the dipole-dipole interaction between the nanowires should be taken into account. Such an approach dealing with *coupled* dipoles is widely used in nanophotonics, particularly, in optics of nanoparticles [23–26]. The concept, basically, consists in finding the values of the dipole moments, acquired by the particles, when each is excited by both the incident (given) field and the sum of the dipole fields from all remaining particles. The dipoles obey the so-called Coupled Dipoles Equation

(CDE):

$$\alpha_i^{-1} \mathbf{d}_i = \sum_{j \neq i} \hat{G}_{ij} \mathbf{d}_j + \mathbf{E}_{0i}, \quad (26)$$

where $\mathbf{E}_{0i} \equiv \mathbf{E}_0(\mathbf{r}_i)$ — the electric field of the incident electromagnetic wave at the point of i -th dipole's location; α_i is the polarizability of i -th particle (the nanowire, in our case); summation is made over the whole ensemble of the wires. The diadic \hat{G}_{ij} is defined through the electric field produced by j -th dipole at point \mathbf{r}_i :

$$E_\alpha(\mathbf{r}_i) = G_{ij,\alpha\beta} d_{j,\beta}, \quad (27)$$

where Greek indices denote Cartesian components. Thus, $\hat{G}_{ij} \mathbf{d}_j$ is the contribution from j -th dipole to the field, acting on i -th one.

After the system of CDE has been solved, any quantity of interest can be found using the values of \mathbf{d}_i . Here we calculate the electric field near the nanowires array, to compare with the results produced by BEM method.

In Fig.6 the squared modulus of the electric field, calculated at the center of the chain of 500 gold nanowires, is plotted for various spacing between them, l , and their radii, a . The exciting field was the plane wave falling by the angle $\theta_1 = \pi/4$ from the left-bottom side (Fig. 1; the polarization is in xy plane; the wavelength is $\lambda = 1512$ nm. As we see, the results of two compared methods perfectly match for 30-nm and 50-nm cylinders, while for the case of 100-nm radius there is a noticeable difference. The discrepancy arise when the diameter, $2a$, becomes comparable with $\lambda/2\pi$, destroying the dipole approximation. Quite remarkable is that such a good agreement between two methods remains up to the gap between the cylinders being as small as their radius.

The computational difficulty of CDE solving rapidly grows with the number of interacting dipoles. However, there is a special case — an infinite chain of dipoles, for which the calculations become drastically more simple. It allows to consider the infinite grating of nanowires analytically, at least for excitation by plane travelling wave.

The main idea is that if the grating of nanowires and the aperture of the incoming wave are both infinite, the wires become fully equivalent. So, the difference in the corresponding dipole moments may originate only from the different values of the incident field at each dipole. In other words, the contribution to the total (acting) field, which is due to dipole-dipole interaction, $\sum_{j \neq i} \hat{G}_{ij} \mathbf{d}_j$, must have the same amplitude at each i -th dipole, and must

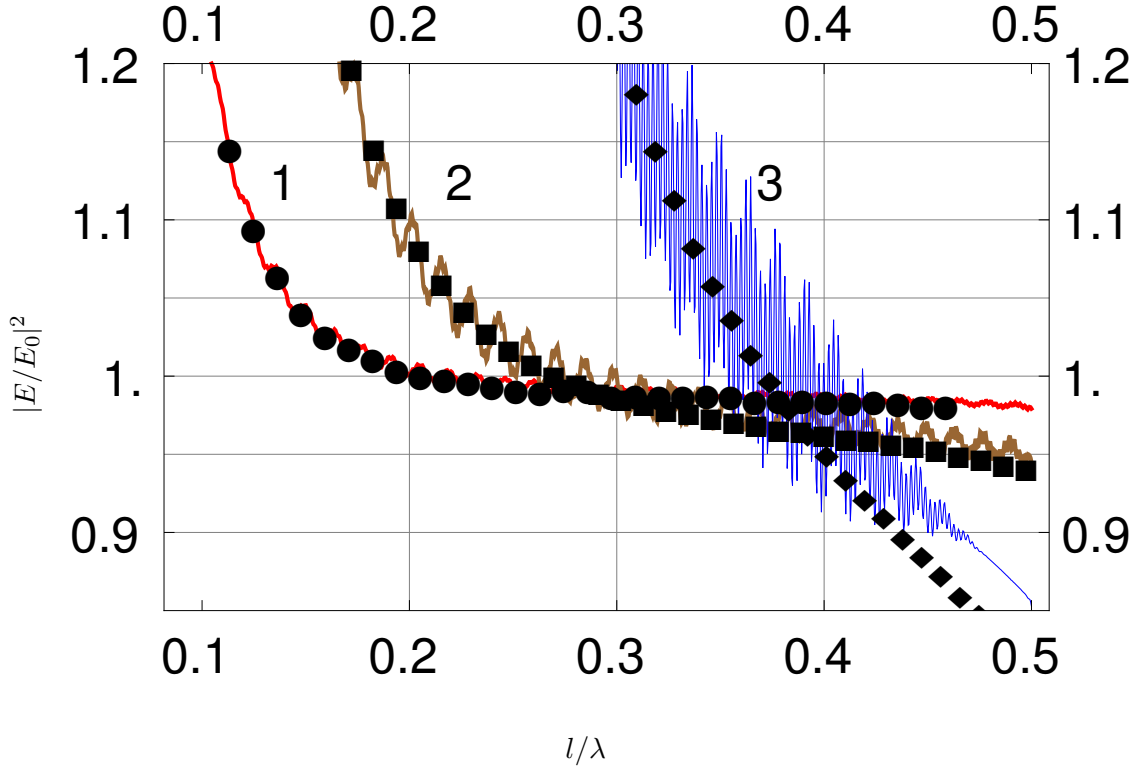


FIG. 6. Comparison of CDE solution for the chain of 500 2D dipoles (solid lines) with that obtained by BEM for the infinite array of nanocylinders (circles and squares). Plotted is the value of squared electric field in the middle of the gap between the cylinders (for CDE, between 250-th and 251-th ones). Here $a = 30$ (curve 1), 50 (2), and 100 nm (3). The field is normalized by the amplitude of the falling wave, E_0 .

be always in phase with the incoming field $\mathbf{E}_0(\mathbf{r}_i)$. Applying these two conditions to (26) we can get an analytical solution of CDE. For this purpose, we use the explicit expression for the electric field of an oscillating 2-dimensional dipole moment $\mathbf{d} \propto \exp(-i\omega t)$

$$\mathbf{E}(\mathbf{r}) = \frac{i\pi k}{r^3} \left[r^2 \mathbf{d} \left(kr \mathcal{H}_0^{(1)}(kr) - \mathcal{H}_1^{(1)}(kr) \right) - \mathbf{r} (\mathbf{d} \cdot \mathbf{r}) \left(kr \mathcal{H}_0^{(1)}(kr) - 2\mathcal{H}_1^{(1)}(kr) \right) \right], \quad (28)$$

which is derived using the approach, very similar to that described in [27] for 3-dimensional case. Also, we use the asymptotic expression for both Hankel functions, that gives an

inaccuracy less than 15% for $kr > 0.5$. After summation we get:

$$d_x = E_0 \alpha \cos \theta_1 \times \quad (29)$$

$$\left\{ 1 - \frac{(1-i)\sqrt{\pi}\alpha}{8\sqrt{kl^5}} [8klF_{3/2} + 3iF_{5/2}] \right\}^{-1},$$

$$d_y = E_0 \alpha \sin \theta_1 \times \quad (30)$$

$$\left\{ 1 - \frac{(1+i)\sqrt{\pi}\alpha}{8\sqrt{kl^5}} [8k^2l^2F_{1/2} + 7iklF_{3/2} - 3F_{5/2}] \right\}^{-1},$$

where

$$F_s \equiv \text{Li}_s(e^{ikl(1-\sin\theta_1)}) + \text{Li}_s(e^{ikl(1+\sin\theta_1)}),$$

$\text{Li}_s(z)$ is the polylogarithm [17]

$$\text{Li}_s(z) = \sum_{n=1}^{\infty} \frac{z^n}{n^s}.$$

The dipole polarizability, α , is the same for all the nanowires; $k = \omega/c$.

The resulting dipole moment d_x is plotted in Fig.7. The calculations were done for gold nanowires with the radius 100 nm as a dependence of the nanowires spacing, at constant wavelength of incoming radiation $\lambda = 1512$ nm. The Rayleigh-Wood's anomalies are clearly seen in Fig. 7 as peaked extrema.

For comparison, we performed also a direct numerical solution of CDE (26) for 500 two-dimensional dipoles, formed by the gold nanowires. The results for d_x component (taken for the "middle" dipole, $i = 250$) are in excellent quantitative agreement with the analytical given above, as also shown in Fig. 7.

The results of the same calculations for d_y are shown in Fig. 8. Comparing to Fig. 7, we see that positions of peaks do not coincide with the case of d_x . It is the shift that produces the splitting shown in Fig. 2. As for the amplitudes difference between analytical and numerical solutions, we believe it to be a consequence of high derivatives near the resonances, that drops down the numerical accuracy.

IV. CONCLUSIONS

An evanescent wave has to be considered together with its source. The special compound Green function is proposed taking into account the falling waves in the lower half space. Boundary integral equations are extended for periodic infinite structure. The effective Green function is found allowing to treat an infinite periodic array of nanowires. The

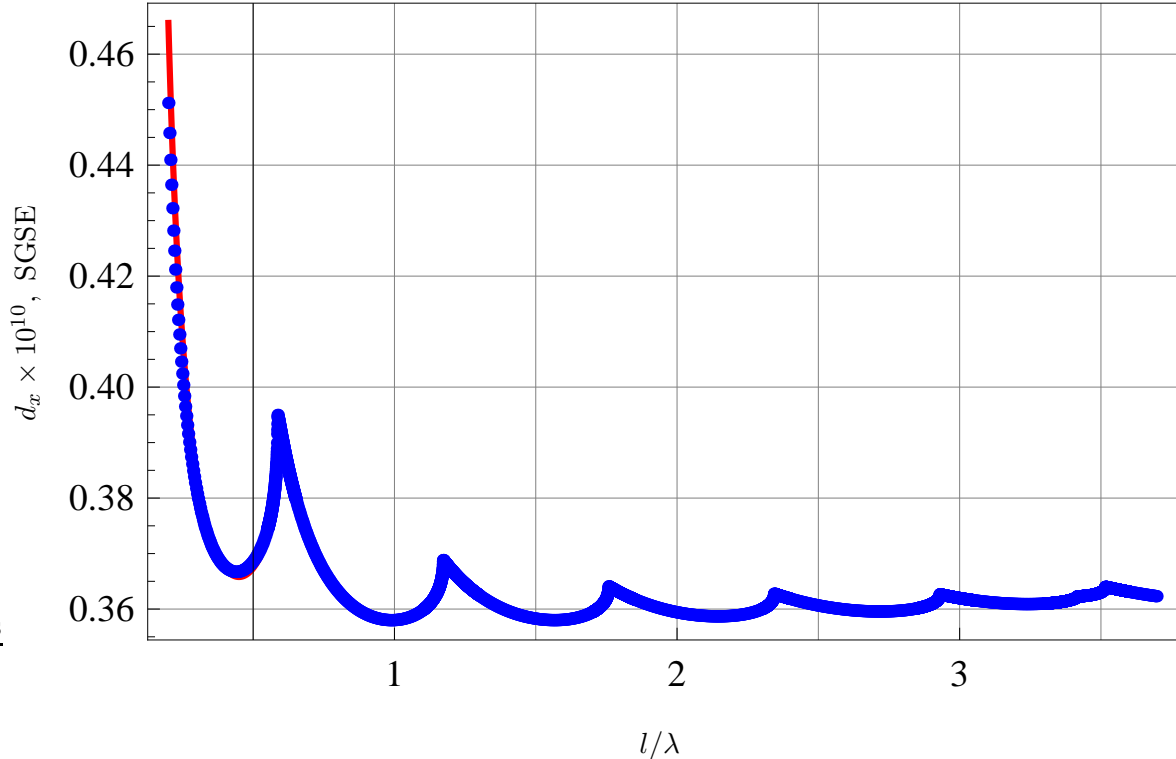


FIG. 7. The absolute value of x-components of the dipole moment d_x vs the relative spacing between the wires, l/λ : the analytical formula for infinite number of wires (solid line); numerical calculation for array of 500 elements (dots).

numerical calculation for circular cylinders reveals Rayleigh — Wood’s anomalies in the grating transparency. The dips turn into peaks and splitting of resonances vanishes when total internal reflection occurs. For the case of evanescent wave nulling the asymptotic value of transparency is shown. The calculations are compared with coupled dipole approximation using the analytical solution, derived for an infinite number of coupled dipoles, and the numerical (direct) calculation for the finite grating with $N = 500$ wires. In the latter case the oscillations are found in the near-field, which are the result of a finite number of cylinders.

ACKNOWLEDGEMENT

Authors are grateful to O. V. Belai and E. V. Podivilov for helpful discussions. This work is supported by the Government program of the leading research schools (NSh-2979.2012.2),

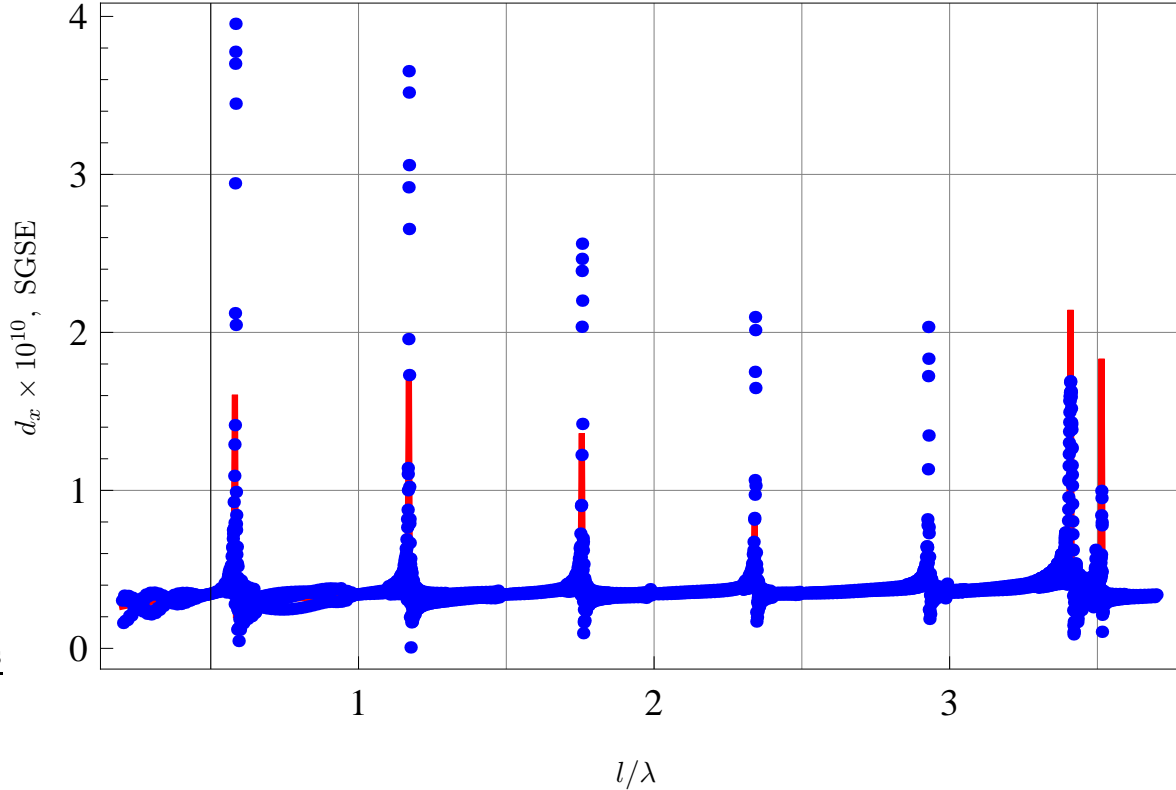


FIG. 8. The same as in Fig.7 for d_y .

program # 24 of the Russian Academy of Sciences Presidium, grant from the Division of Physical Sciences, and Interdisciplinary grant #68 from the Siberian Branch of RAS.

-
- [1] D. W. Pohl, W. Denk, and M. Lanz, *Appl. Phys. Lett.* **44**, 651 (1984).
 - [2] C. M. Winterflood, T. Ruckstuhl, D. Verdes, and S. Seeger, *Phys. Rev. Lett.* **105**, 108103 (2010).
 - [3] A. Bialiyeu, A. Bottomley, D. Prezgot, A. Ianoul, and J. Albert, *Nanotechnology* **23**, 444012 (2012).
 - [4] R. F. Harrington, *Time-Harmonic Electromagnetic Fields* (Wiley, NewYork, 2001).
 - [5] S. V. Zymovetz and P. I. Geshev, *Technical Physics* **51**, 291 (2006).
 - [6] O. V. Belai, L. L. Frumin, S. V. Perminov, and D. A. Shapiro, *Opt. Lett.* **36**, 954 (2011).
 - [7] O. V. Belai, L. L. Frumin, S. V. Perminov, and D. A. Shapiro, *EPL* **97**, 10007 (2012).

- [8] K. Busch, G. von Freymann, S. Lindenb, S. F. Mingaleeva, L. Tkeshelashvilia, and M. Wegener, *Phys. Rep.* **444**, 101202 (2007).
- [9] F. J. Garcia de Abajo, *Rev. Mod. Phys.* **79**, 1267 (2007).
- [10] F. Flory, L. Escoubas, and G. Berginc, *J. Nanophoton.* **5**, 052502 (2011).
- [11] J. Arlandis, E. Centeno, R. Pollès, A. Moreau, J. Campos, O. Gauthier-Lafaye, and A. Monmayrant, *Phys. Rev. Lett.* **108**, 037401 (2012).
- [12] V. M. Shalaev, W. Cai, U. K. Chettiar, H.-K. Yuan, A. K. Sarychev, V. P. Drachev, and A. V. Kildishev, *Opt. Lett.* **30**, 3356 (2005).
- [13] C. A. Brebbia, J. C. F. Telles, and L. C. Wrobel, *Boundary element techniques* (Springer, Berlin, 1984).
- [14] T. W. Wu, ed., *Boundary Element Acoustics: Fundamentals and Computer Codes* (WIT Press, Southampton, 2000).
- [15] G. Beer, I. Smith, and C. Duenser, *The Boundary Element Method with Programming: For Engineers and Scientists* (Springer, Berlin, 2008).
- [16] M. Born and E. Wolf, *Principles of optics; electromagnetic theory of propagation, interference and diffraction of light* (Pergamon Press, Oxford — New York, 1965).
- [17] F. W. J. Olver, D. W. Lozier, R. F. Boisvert, and C. W. Clark, *NIST Handbook of Mathematical Functions* (Cambridge University Press, New York, 2010).
- [18] L. M. Brekhovskikh, *Waves in layered media* (Academic Press, New York, 1980).
- [19] L. D. Landau and E. M. Lifshitz, *Fluid Mechanics*, Course of Theoretical Physics, Vol. 6 (Pergamon, New York, 1959).
- [20] F. Pincemin, A. Sentenac, and J.-J. Greffet, *J. Opt. Soc. Am. A* **11**, 1117 (1994).
- [21] J.-J. Greffet, *Opt. Commun.* **72**, 274 (1989).
- [22] We assume the absolute convergence of the corresponding series.
- [23] E. M. Purcell and C. R. Pennipacker, *Astrophys. J.* **186**, 705 (1973).
- [24] V. A. Markel, L. A. Muratov, M. A. Stockman, and T. F. George, *Phys. Rev. B* **43**, 8183 (1991).
- [25] M. I. Stockman, *Phys. Rev. E* **56**, 6494 (1997).
- [26] S. V. Perminov, S. G. Rautian, and V. P. Safonov, *Opt. Spekt.* **95**, 416 (2003).
- [27] L. D. Landau and E. M. Lifshitz, *The Classical Theory of Fields*, Course of Theoretical Physics, Vol. 2 (Pergamon, New York, 1951).